X2 VVER-1000 benchmark revision: fresh HZP core state and the reference Monte Carlo solution

Bilodid, Y.; Fridman, E.; Lötsch, T.;

Originally published:

May 2020

Annals of Nuclear Energy 144(2020), 107558

DOI: https://doi.org/10.1016/j.anucene.2020.107558

Perma-Link to Publication Repository of HZDR:

https://www.hzdr.de/publications/Publ-29992

X2 VVER-1000 benchmark revision: fresh HZP core state and the reference Monte Carlo solution

Yuri Bilodid[1,a], Emil Fridman[1], Thomas Lötsch[2]

[1]Helmholtz-Zentrum Dresden-Rossendorf
Dresden, Germany

[2]TÜV SÜD Industrie Service GmbH
Munich, Germany

Abstract

The X2 VVER-1000 benchmark provides a unique set of the operational data of a VVER-1000 reactor. This includes fresh core hot zero power (HZP) experiments, operational history of first four fuel cycles, and information on the operational transients occurred on the unit during first cycles. Since a publication of the initial versions of the benchmark, numerous updates, corrections and refinements become available.

The current paper is a first in a series of publications on the revised X2 VVER-1000 benchmark. It is dedicated to the fresh core HZP experiments and includes description of fuel and core geometries, the material compositions, description and results of measurements taken during fresh core start-up. In addition, the paper includes the reference Monte Carlo solution for the HZP experiments obtained with Serpent 2. The calculated and measured values are in a good agreement. Further extension of the benchmark definition is foreseen in the near future.

Keywords: X2 benchmark, VVER-1000, Serpent.

1 Introduction

The reactor simulation tools are under continuous development and improvement and a crucial part of this process is verification and validation (V&V). On one hand, code-to-code verification, numerical benchmarks, and experiments on dedicated facilities provide clearly defined problems and are very useful for testing single methods and models. On the other hand, the validation against real power plant measurements allows testing integral performance of a code, its ability to predict reactor parameters and often is a necessary requirement for tools used for safety analysis. The publicly available data for such validation, particularly for VVER-1000 reactors, is very limited. The OECD NEA benchmarks Kalinin-3 (Tereshonok et al., 2009) and Kozloduy-6 (Ivanov et al., 2002) describe VVER-1000 operational transients, but their specifications missing of fuel geometry and materials definitions and fuel cycle operational data, providing libraries of homogenised fuel properties instead.

During the 19th and 20th AER Symposium ("AER," 2019) in 2009 and 2010, a new VVER-1000 core benchmark was proposed (Lötsch et al., 2009, 2010). The benchmark was based on the VVER-1000 operational data of the second unit of the Khmelnitsky Nuclear Power Plant (NPP) located in Ukraine. The unit was put in

[a]Corresponding author. E-mail: y.bilodid@hzdr.de

operation in 2004 and was one of first VVER-1000 unit fully loaded with fresh TVSA fuel type. The benchmark was called “X2” where “X” stands for “Kh” in Ukrainian transcription and “2” stands for the unit number.

The X2 benchmark specifications comprise a unique set of the VVER-1000 plant data such as a detailed core definition, operational history of the first four fuel cycles, various measurement results, and description of several operational transients (Lötsch et al., 2016). The goal of the benchmark is to provide best available information for V&V of reactor simulators applied to VVER analyses. For instance, the measured data such as critical boron concentration during fuel cycles, reactivity coefficients, control rod worth, and self-powered neutron detectors (SPND) readings can be directly compared with calculated values. For values that are not measured, such as pin power distribution or spent fuel isotopic content, the higher order solutions based on Monte Carlo could be used as a reference.

The benchmark is logically divided into three parts with a growing level of simulation complexity:

- Fresh core hot zero power (HZP) experiments;
- The depletion part containing core layouts and operational history of first four fuel cycles as well as measured power distribution snapshots for selected time points of each cycle.
- The transient part containing documented information on the operational transients occurred at the unit during first cycles such as reactor SCRAM, xenon oscillations, and a main coolant pump trip.

In the previous years, the X2 benchmark was partially solved applying combination of lattice transport and nodal diffusion codes (Lötsch et al., 2012, 2013). The Monte Carlo code Serpent was used for fuel assembly depletion analysis in (Lötsch, 2014) and (Novak et al., 2017). The benchmark data was also recently used for testing of newly developed tools (Bahadir, 2018; Bilodid et al., 2018). Since a publication of the initial versions of the benchmark, numerous updates, corrections and refinements are become available. These served as an incentive for updating the specifications and issuing a revised version of the X2 benchmark.

The current paper is a first part in a series of publications on the revised X2 VVER-1000 benchmark. It is dedicated to the fresh core HZP experiments and includes description of fuel and core geometries, definition of the material compositions, description and results of measurements taken during fresh core start-up. In addition, the paper includes the reference Monte Carlo solution for the HZP experiments obtained with Serpent 2 (Leppänen et al., 2015).

Main refinements of the presented benchmark revision in comparison to the initial definition (Lötsch et al., 2009, 2010) are:

- The radial reflector specification is replaced by realistic heterogeneous from (Krýsl et al., 2016);
- The axial reflector specifications are replaced by more realistic ones;
- Added geometry illustration for main model components;
- Corrected specification of the dysprosium titanate used as an absorber in the control rods;
- All material compositions are provided as nuclide number densities;
- Corrected definition of a control rod axial position;
- Description of a start-up test procedures;
- Revised values of the fresh core HZP temperature reactivity coefficients;

Moreover, in order to facilitate the modelling process, the benchmark definition is supplemented with digital data such as high resolution geometry images of the main core components, spreadsheets with operational data and material compositions, etc.

The benchmark definition will be complemented with the depletion and the transient parts as near future work. The depletion part contains core layouts and operational history of four first fuel cycles as well as measured power distribution snapshots for selected moments in each cycle. The transient part contains

operational transient occurred and documented on the unit during first cycles: reactor SCRAM, xenon oscillation and a main coolant pump trip.

The benchmark definition and associated data package are hosted online at the HZDR data repository website https://doi.org/10.14278/rodare.199, where future revisions of the benchmark specification will be made publicly available.

2 Benchmark specification

This chapter provides a detailed description of the benchmark specification. The following information is provided.

- Geometry description of the fuel assemblies, axial and radial reflectors,
- Material specifications of fuel and structural materials,
- Description of the plant operational data and the measurement data for the HZP start-up tests.

It should be noted that the bulky data tables and high-resolution images are provided in an embedded dataset.

2.1 Core geometry

2.1.1 Fuel assembly

The TVSA hexagonal fuel assembly (FA) design, fabricated by the Russian "TVEL" Fuel Company, was utilised in the described reactor core. The distinguishing features of the TVSA design are the introduction of the stiffening plates in assembly corners to improve mechanical stability and the use of gadolinium as a burnable absorber.

TVSA radial plan geometry is described in Fig. 2.1 and Table 2.1. Fig. 2.2 shows geometry of a corner stiffener. All dimensions are provided at room temperature (20°C).

Eight types of TVSA fuel assemblies with different enrichment and number of burnable absorber (BA) pins are described in Table 2.2 and Fig. 2.8-Fig. 2.14. Only first five fuel assembly types were used in the first fuel cycle (see Table 2.7), while other were loaded in later cycles.

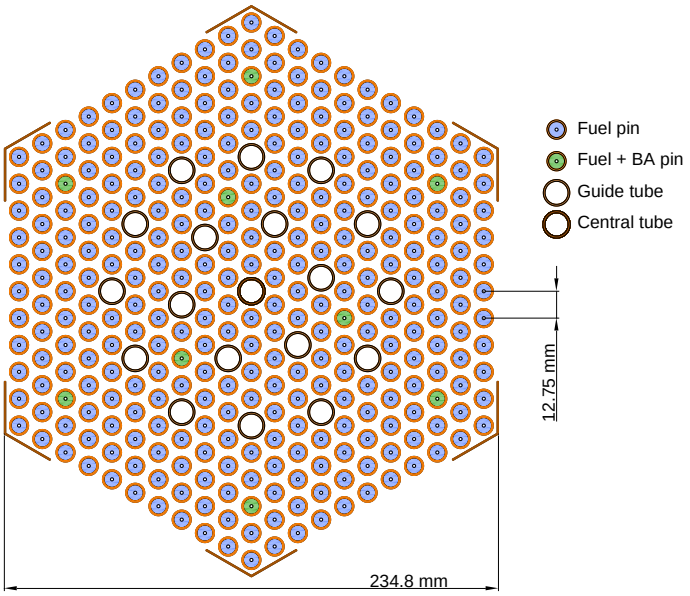

Fig. 2.1 Fuel assembly geometry

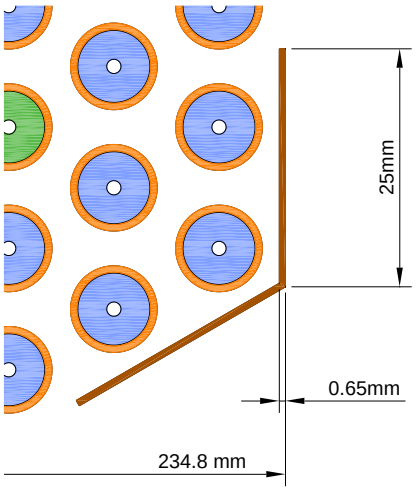

Fig. 2.2 Corner stiffener geometry

Table 2.1 TVSA design

Parameter	Value
Fuel assembly	
Assembly lattice pitch in the core, cm	23.6
Flat-to-flat assembly size, cm	23.48
Rod lattice pitch, cm	1.275
Active height, cm	353
Number of fuel pins	312
Number of guide tubes	18
Number of central tubes	1
Mass of fuel (UO_2 + Gd_2O_3) in assembly, kg	491.4±4.5
Corner stiffener	
Number of corner stiffeners in FA	6
Width of one plate, cm	2.5
Thickness, cm	0.065
Material	alloy E635
Mass of one corner stiffener, kg	1.4

Fig. 2.3 shows radial geometry of a fuel pin. All fuel pins, including burnable absorbers, have a central hole. The central hole and a gas gap between fuel pellet and cladding are filled with helium. Fig. 2.4 shows radial geometry of a fuel pin lower plug and Fig. 2.5 shows radial geometry of a fuel pin upper plenum (see section 2.1.2).

Fig. 2.6 shows radial geometry of a guide tube with inserted control rod. In absence of control rod, the guide tube is filled with coolant. Fig. 2.7 shows radial geometry of a central tube filled with coolant.

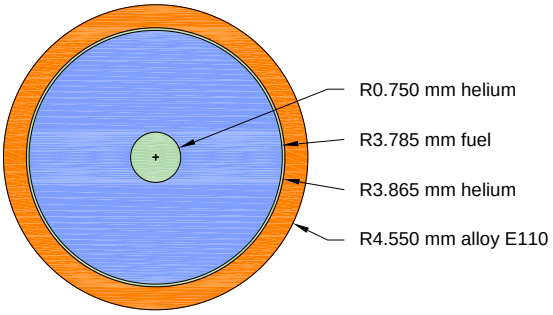

Fig. 2.3 Fuel pin

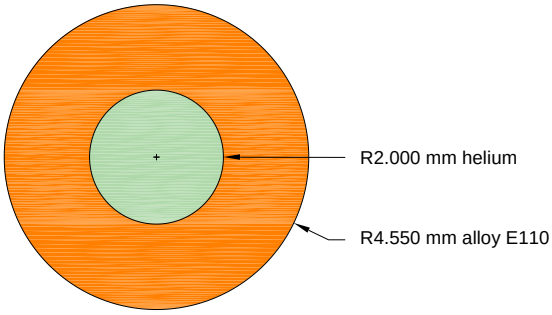

Fig. 2.4 Fuel pin lower plug

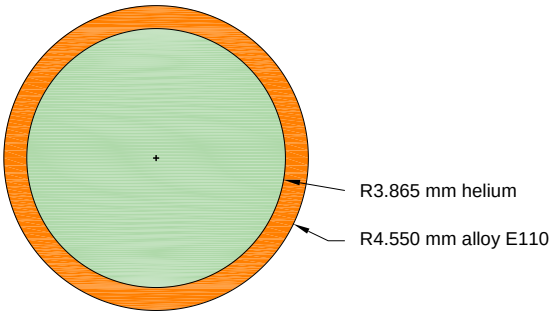

Fig. 2.5 Fuel pin upper plenum

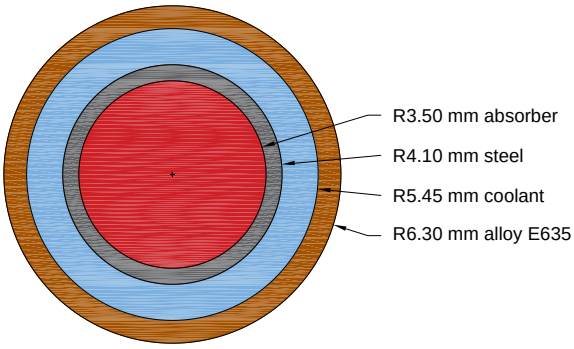

Fig. 2.6 Guide tube with control rod

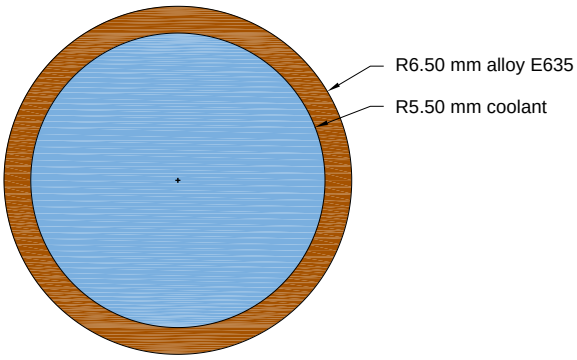

Fig. 2.7 Central tube geometry

Table 2.2 TVSA fuel types

FA Type	No. of fuel pins / enrichment	Number of Gd-pins (w% Gd_2O_3/^{235}U)
13AU	312 / 1.30	--
22AU	312 / 2.20	--
30AV5	303 / 3.00	9 (5.0/2.4)
39AWU	243 / 4.00 60 / 3.60	9 (5.0/3.3)
390GO	240 / 4.00 66 / 3.60	6 (5.0/3.3)
398GO	306 / 4.40	6 (5.0/3.3)
430GO	240 / 4.40 66 / 4.00	6 (5.0/3.6)
439GT	306 / 4.40	6 (5.0/3.6)

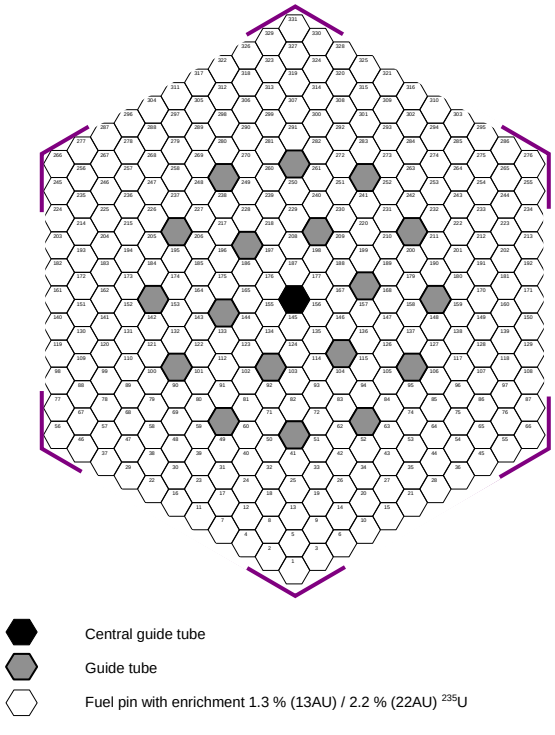

Fig. 2.8 Pin layout of fuel assembly types 13AU and 22AU

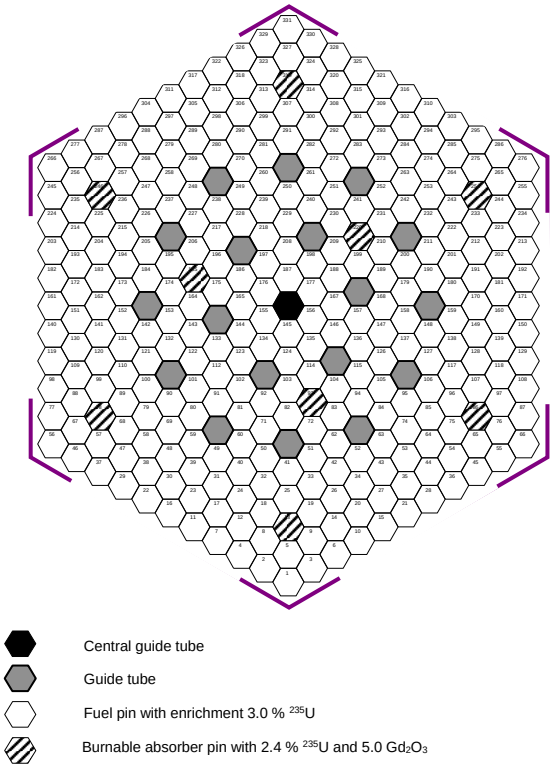

Fig. 2.9 Pin layout of fuel assembly type 30AV5

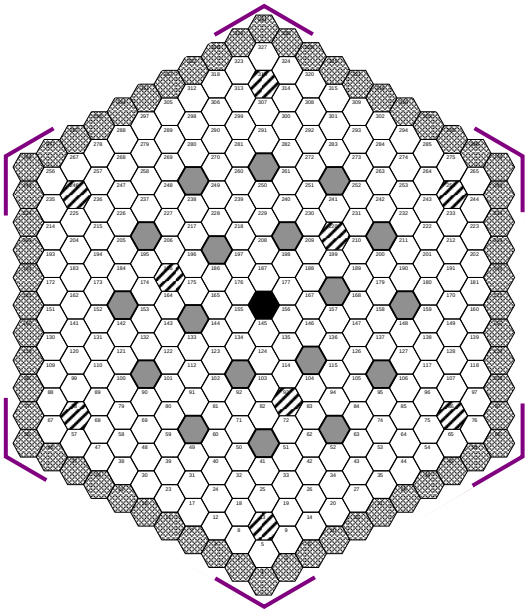

Central guide tube

Guide tube

Fuel pin with enrichment 4.0 % ^{235}U

Fuel pin with enrichment 3.6 % ^{235}U

Burnable absorber pin with 3.3 % ^{235}U and 5.0 % Gd_2O_3

Fig. 2.10 Pin layout of fuel assembly type 39AWU

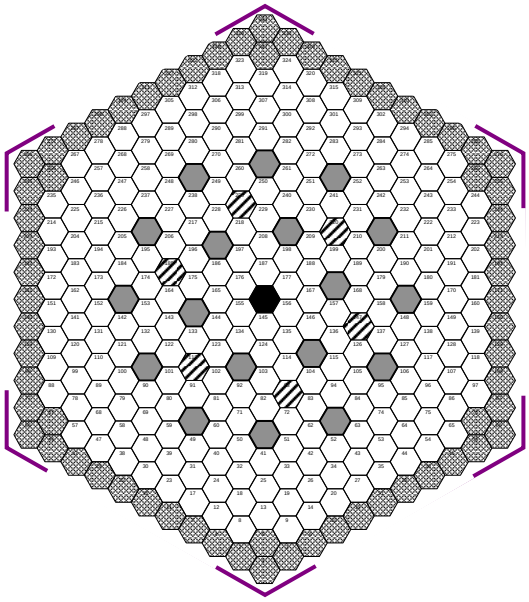

Central guide tube

Guide tube

Fuel pin with enrichment 4.0 % ^{235}U

Fuel pin with enrichment 3.6 % ^{235}U

Burnable absorber pin with 3.3 % ^{235}U and 5.0 Gd_2O_3

Fig. 2.11 Pin layout of fuel assembly type 390GO

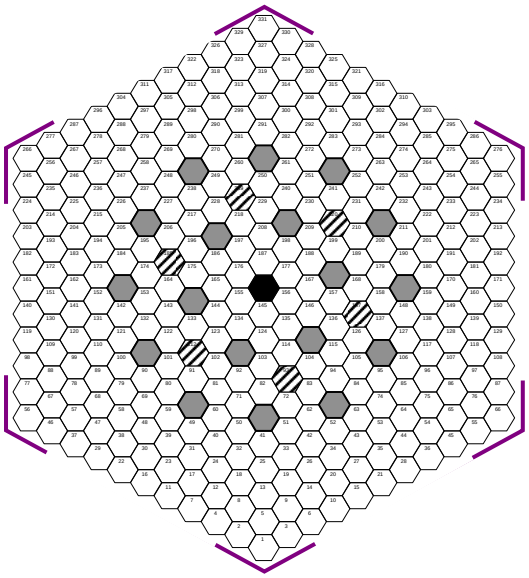

Central guide tube

Guide tube

Fuel pin with enrichment 4.0 % ^{235}U

Burnable absorber pin with 3.3 % ^{235}U and 5.0 Gd_2O_3

Fig. 2.12 Pin layout of fuel assembly type 398GO

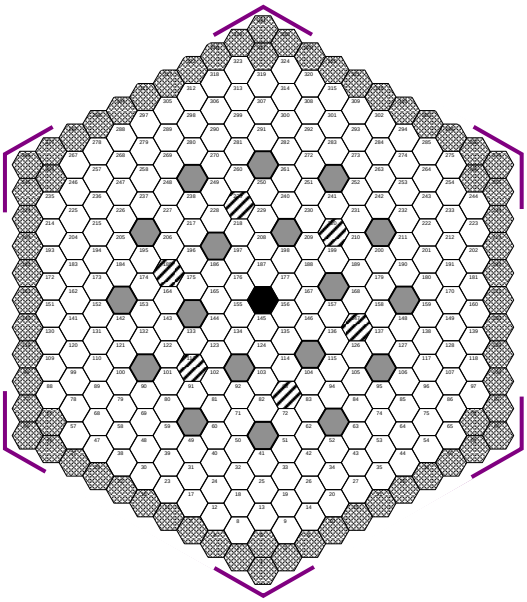

Central guide tube

Guide tube

Fuel pin with enrichment 4.4 % ^{235}U

Fuel pin with enrichment 4.0 % ^{235}U

Burnable absorber pin with 3.6 % ^{235}U and 5.0 Gd_2O_3

Fig. 2.13 Pin layout of fuel assembly type 430GO

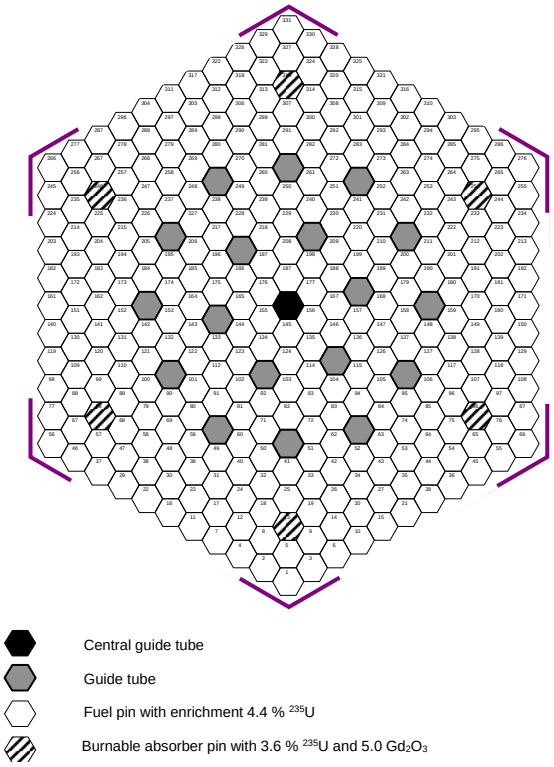

Fig. 2.14 Pin layout of fuel assembly type 439GT

2.1.2 Axial geometry

Fig. 2.15 demonstrates axial layout of the proposed model (please note that horizontal and vertical axes are not in the same scale). Axial layers form bottom to top are: two lower homogeneous mixture layers, fuel pin lower plug, fuel region (see Fig. 2.3), upper plenum and two upper homogeneous layers. The compositions of homogeneous mixture layers are shown in Table 2.5. The fuel height in a cold state is 353 cm. However, in the proposed model the fuel height of 355 cm is used as a simple approximation of axial thermal expansion.

Fuel assembly contains 14 spacer grids, located with an axial pitch 255 mm starting from the bottom of fuel. Each spacer grid has 20 mm width and contain 0.55 kg of alloy E110. In the shown model spacer grids are modelled as additional thickness of a fuel cladding preserving alloy mass.

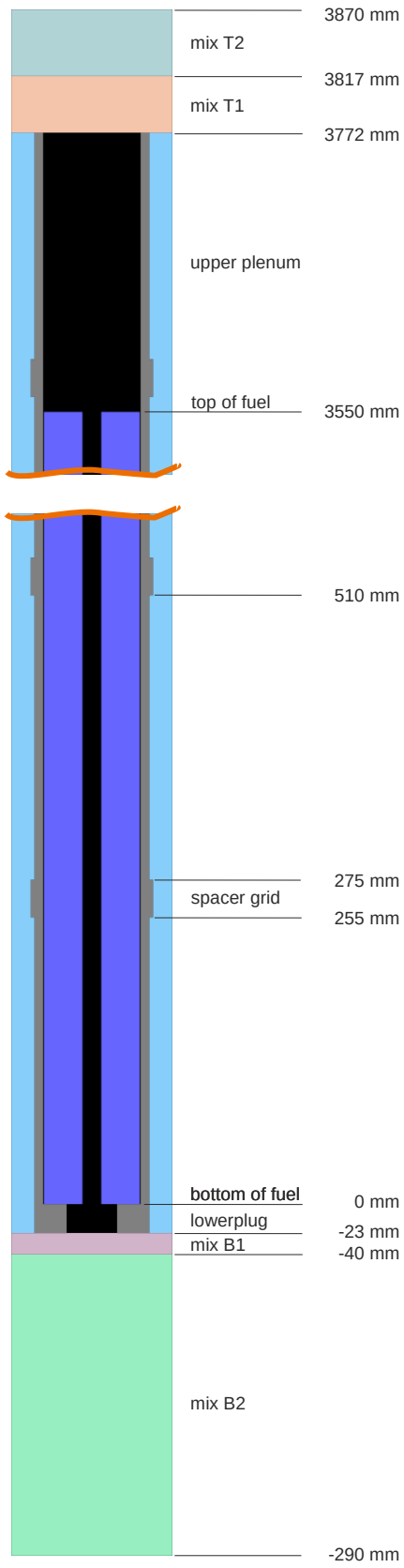

Fig. 2.15 Axial layout of the fuel pin model

2.1.3 Radial reflector

The dimensions and structure of a radial reflector are shown in Fig. 2.16. The reflector is 30° symmetric. Reflector structures (in order from core center to periphery) are core basket with coolant channels and "groove" region, coolant gap, core barrel, coolant downcomer, and reactor pressure vessel (RPV). Table 2.3 provides coordinates of basket coolant channels relatively to the center of the core.

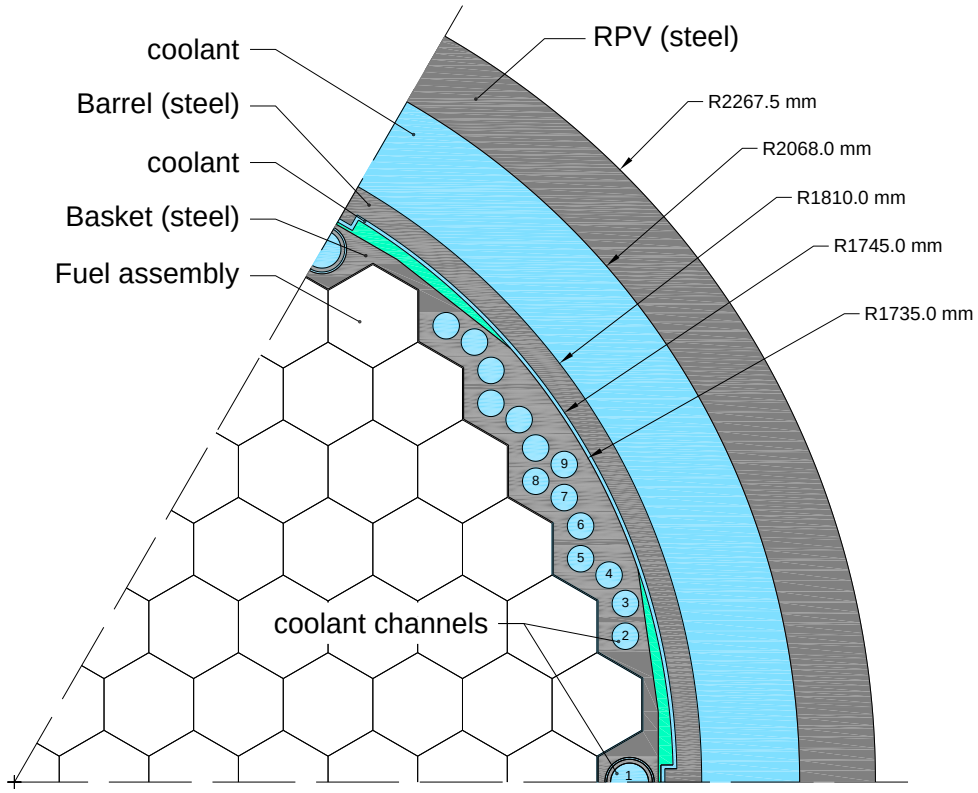

Fig. 2.16 Radial reflector

Table 2.3 Basket coolant channels: coordinates and dimensions

Number	X, mm	Y, mm	Diameter, mm
1	1620	0	130
2	1609	384	70
3	1609	470	70
4	1566	545	70
5	1491	588	70
6	1491	674	70
7	1448	749	70
8	1373	792	70
9	1448	836	70

The geometry details of the core basket are shown in Fig. 2.17. It should be noted that there is an additional 3 mm gap, filled with coolant, between fuel assembly lattice (with 236 mm pitch) and the core basket. The basket coolant channel #1 has a steel tube inside and gaps are filled with coolant. The outer surface of the core basket is cylindrical with horizontal grooves. For model simplification, the grooves region is described by a homogeneous mixture of coolant and steel (material "Groove" in Table 2.5). As another simplification, the radial reflector geometry in the proposed model does not change in axial direction.

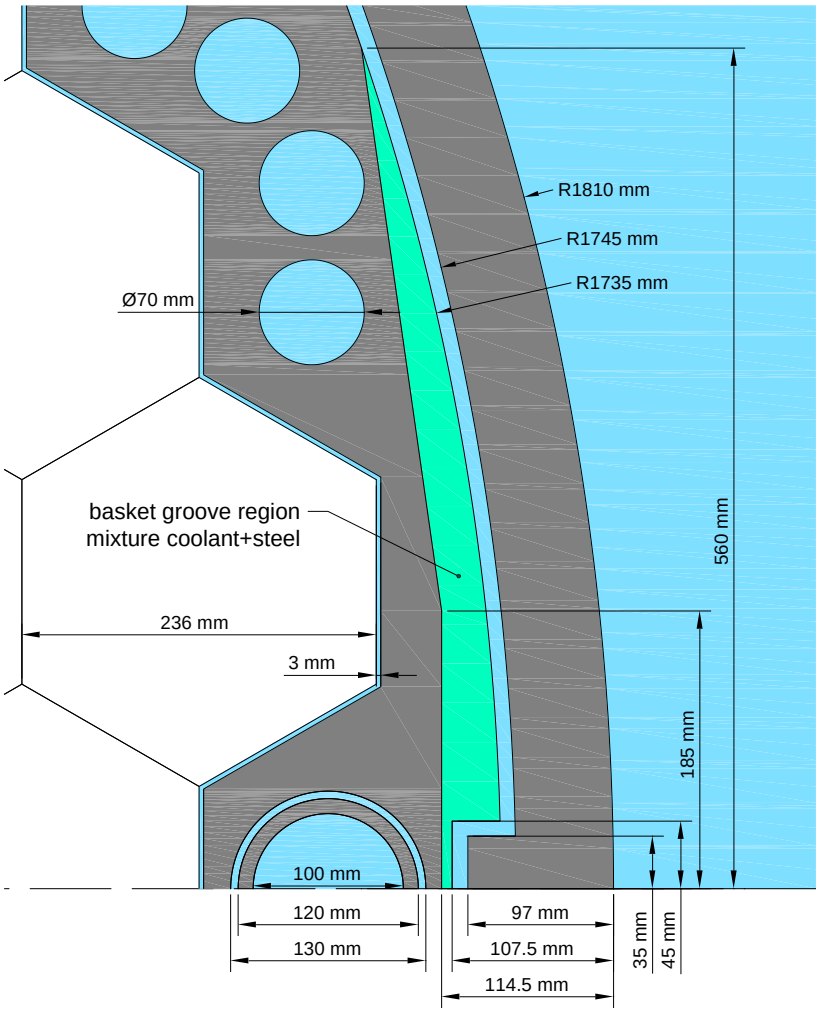

Fig. 2.17 Core basket details

2.2 Control rods

The individual control rod is a steel tube filled with absorber material (see Fig. 2.6). The total length of the absorbing part is 3500 mm, from which lower 300 mm are filled with dysprosium titanate and upper 3200 mm with boron carbide. 18 individual control rods are fixed in a control rod cluster, which could be inserted into corresponding guide tubes of a fuel assembly. Total 61 control rod clusters are combined in 10 banks as shown in Fig. 2.18. Bank number #10 is routinely used for criticality control during normal operation

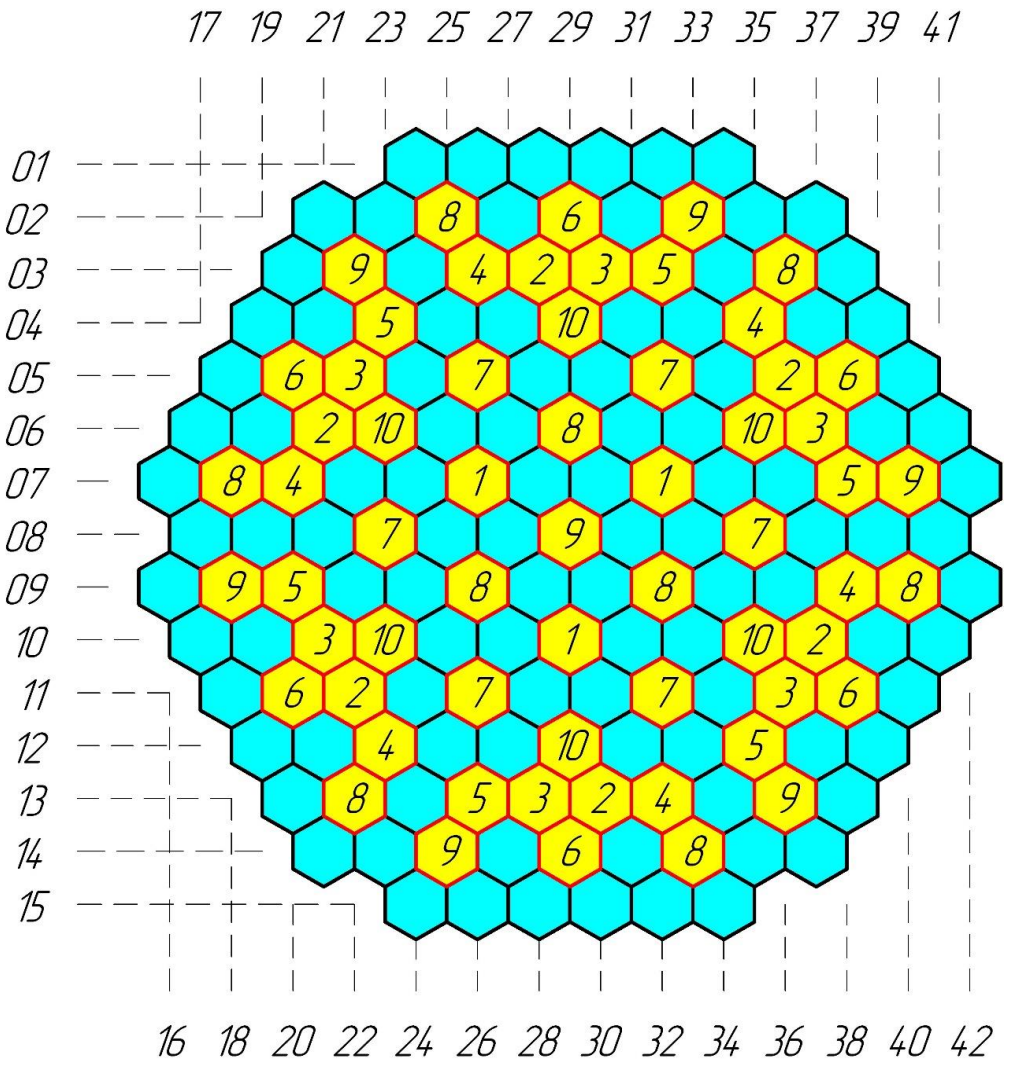

Fig. 2.18 Positions of the control rod banks in the reactor core

Axial position of control rod banks H_i ***[%]*** is provided in operational data in per cent of withdrawal, where 0% means control rod is fully inserted and 100% is fully withdrawn. The distance ***h [cm]*** between lower edge of absorber rod and bottom of the fuel (in cm) can be calculated as follows:

$$h = H \times \frac{350}{100} + 14$$

where ***H*** is axial position in % as provided in operational data.

2.3 Material definition

The compositions of all fuel and structural materials are provided in the embedded dataset in a form of isotopic number densities. These isotopic number densities were derived applying natural abundances and considering the assumptions presented below.

Fuel materials

The material of fuel pellets in fuel rods is enriched uranium dioxide UO_2, while material of fuel pellets in burnable absorber rods is a mixture of enriched UO_2 with 5 weight % of Gd_2O_3.

The effective UO_2 density was estimated as a ratio between mass and volume of UO_2 in a fuel rod. The assumed UO_2 mass was 491.4 kg per assembly or 1575 g per fuel rod. The fuel rod dimensions are shown in Table 2.1 and Fig. 2.3, thermal expansions in a radial direction are ignored. The fuel column active length in a cold state is equal to 353 cm, but it was assumed to be 355 cm as a simple approximation of thermal expansion. The calculated effective UO_2 density is 10.2605 g/cm^3.

The effective density of the $UO_2 + Gd_2O_3$ mixture in burnable absorbers was calculated assuming mass of mixture per rod equal to 1570 g and the same fuel rod dimensions as described above. The calculated effective $UO_2 + Gd_2O_3$ mixture density is 10.2279 g/cm^3.

The effective calculated densities were used to derive atomic number densities of the fuel and the burnable absorber rods.

Structural materials

The considered structural materials include two zirconium alloys (E110 and E635), steel and control rod absorbers. The main upper part of the control rod absorber consists of boron carbide B_4C while the lower part consists of dysprosium titanate $Dy_2O_3 \cdot TiO_2$. The elemental compositions of structural materials used for calculation of isotopic number densities are summarized in Table 2.4.

Table 2.4 Composition of structural materials

Alloy E110		Alloy E635		Steel		$Dy_2O_3 \cdot TiO_2$		B_4C	
Element	**wt.%**	**Element**	**wt.%**	**Element**	**wt.%**	**Element**	**wt.%**	**Element**	**wt.%**
Zr	98.97	Zr	98.47	Fe	69.50	O	18.00	B-10	14.43
Nb	1.00	Nb	1.00	Cr	18.00	Ti	12.00	B-11	63.84
Hf	0.03	Fe	0.50	Ni	11.00	Dy	70.00	C	21.74
		Hf	0.03	Mn	1.50				
Density, g/cm^3	6.4516		6.5500		7.900		5.1000		1.800

Reflector homogeneous mixtures

The axial reflectors layers (Fig. 2.15) and core basket groove region (Fig. 2.17) are modelled by homogeneous mixture materials. Table 2.5 provides volumetric composition of the mixtures. The coolant material in each mixture should correspond to the local state – i.e. boric acid concentration, temperature and density of core inlet and outlet.

Table 2.5 Composition of homogeneous mixtures

Mixture	B1	B2	T1	T2	Groove
Material			**Volumetric part, %**		

Mixture	B1	B2	T1	T2	Groove
Material	**Volumetric part, %**				
Coolant	57	67	56	98.9	34.5
Steel	33	33	1.9	0	65.5
Alloy E635	10	0	30.6	1.1	0
helium	0	0	11.5	0	0

2.4 Operational data

This chapter provides the operational data of the Unit 2 and describes the conducted start-up tests. The legend for data provided in tables of this chapter:

Table 2.6 Operational data description

Data column	Data legend	Accuracy
H_*X*, %	Position of the control rod bank #*X* in %	±1 %
CB, g/kg	Boric acid (H_3BO_3) concentration in gram of acid per kilogram of coolant	±2 %
Tin, °C	Core inlet coolant temperature	<±1 °C
P, MPa	Pressure above the reactor core	
Nth, MW	Thermal power of the reactor core	±2 %
G, m3/h	Volumetric coolant flow rate through the reactor, including bypasses	

The accuracy of each parameter measurement is not known exactly. Nevertheless, a nominal measurement accuracy of some parameters is provided.

The boric acid concentration is provided in g/kg (gram of acid per kilogram of coolant) units, which are commonly used for VVER reactors. It could be recalculated into ppm units, which are common for PWR, using the following expression:

$$CB, ppm = 174.88 \times CB, g/kg.$$

2.4.1 Core layout

The fuel loading pattern for the 1st cycle is shown in Fig. 2.19. The loaded TVSA fuel types are listed in Table 2.7. All fuel assemblies are fresh.

Table 2.7 1st fuel cycle fuel inventory

FA Type	No. of FA in the core	Residence time, years
13AU	48	0
22AU	42	0
30AV5	37	0
39AWU	24	0
390GO	12	0

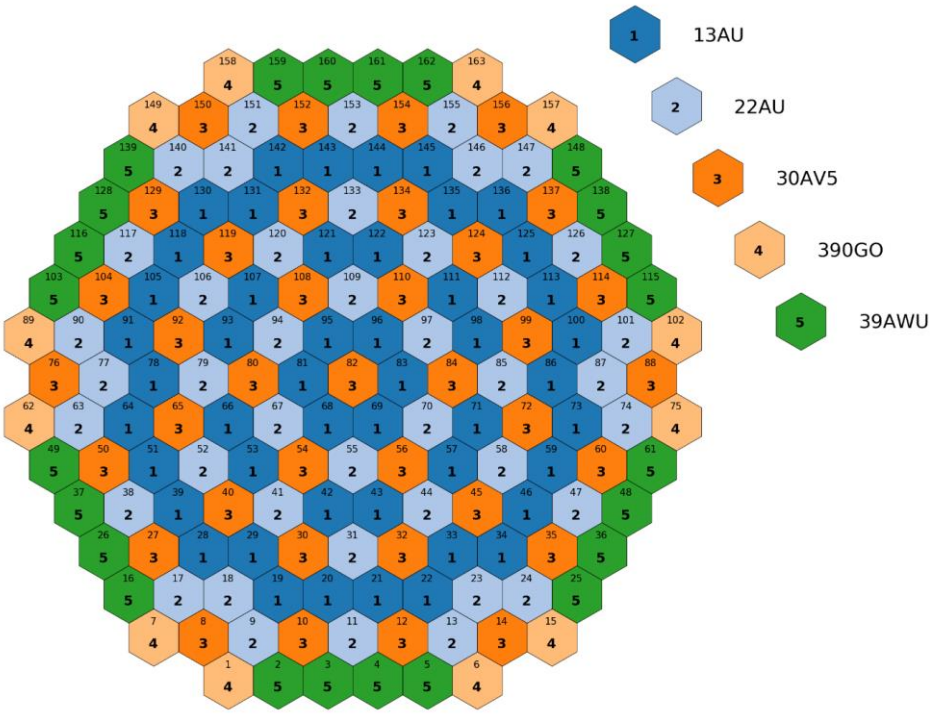

Fig. 2.19 Core layout of the 1st fuel cycle

2.4.2 HZP start-up tests at the fresh core

Standard tests, such as measurement of temperature reactivity coefficients and control rod worth are performed on HZP at the start-up of each fuel cycle. Measurement results and their uncertainties were estimated by NPP staff and provided here as specified in the NPP reports.

Critical state

Measurement procedure starts after reactor reaches a stable state, which means stable levels of operational parameters such as boric acid concentration, pressuriser water level, etc. The critical conditions are summarized in Table 2.8.

Table 2.8 Critical state

H10, %	H1-9, %	CB, g/kg	Tin, °C	P, MPa
76	100	6.9	281.0	15.76

Temperature reactivity coefficient

The measurements of temperature reactivity coefficient were conducted at HZP, zero-burnup state (no fission product poisoning, no Xe135, no Sm149), and with the fully withdrawn (H=100%) control rods in banks 1 to 6.

In order to measure the temperature reactivity coefficients, the core inlet coolant temperature was first (slowly) decreased and then increased back by varying the steam flow rate from the steam generator. The measurement procedure was repeated for two different CB concentrations. Reactivity insertion due to the coolant temperature change was compensated by control rod movements. The position of control rods in banks 7-10, operating conditions and the measured temperature reactivity coefficient are presented in Table 2.9.

Reactivity was measured by a "reactimeter" measuring device. It is connected to the outer-core ionisation chambers and obtains as an input an electrical signal, proportional to a neutron flux level. The signal is converted into reactivity (in $ units) by inverse point kinetics using a provided value of effective delayed neutron fraction (βeff). The value of ßeff used in these measurements is equal to 730 pcm.

Table 2.9 Measurements of the temperature reactivity coefficients

H10, %	H9, %	H8 %	H7 %	CB, g/kg	Tin, °C	P, MPa	Δρ/ΔT, pcm/°C
76	100	100	100	7.05	280.7-276.0	15.76-15.74	-4.88±0.50
					276.4-280.6	15.74-15.67	-5.39±0.54
0	0	31	80	5.70	280.3-275.7	15.82-15.82	-13.58±0.14
					275.7-280.2	15.82-15.82	-14.67±0.15

SCRAM worth

The SCRAM worth was measurement in two steps.

- First, from the nearly critical state all control rods, except the chosen "stuck" cluster, were dropped to the lowest position. The worth of SCRAM with one cluster "stuck" was measured.
- Second, after about 1 minute the "stuck" rod was dropped down and the full SCRAM worth was measured.

The coolant temperature and boric acid concentration remained practically unchanged during the SCRAM test. The control rod cluster in fuel assembly #17 from the control rod bank 8 (coordinates 13-22 in Fig. 2.18) was chosen to simulate the "stuck" rod. The position of control rods, operating conditions, and the measured SCRAM worth are presented in Table 2.10.

Table 2.10 Measurements of the SCRAM worth

Reactor state	H10, %	H1-9, %	H_#17 %	CB, g/kg	Tin, °C	P, MPa	SCRAM worth, $
Before SCRAM	75	100	100	6.9	280.5	15.66	-
SCRAM with #17 at 100%	0	0	100				5.23±0.31
Full SCRAM	0	0	0				7.00±0.43

The integral and differential worth of control rod bank #10

The integral and differential worth of control rod bank #10 was measured according to the following procedure. Initially, the control rod bank #10 was fully inserted while all other control rod banks were fully

withdrawn. During the measurements, the boron concentration in coolant has been constantly increased, inserting negative reactivity. To keep reactor critical, the control rod bank #10 was step-wise withdrawn, with steps length of 4-7%. The introduced positive reactivity on each step **Δρ** was measured by reactimeter. The core inlet coolant temperature and pressure above the core were kept stable during the measurements.

The measured values are shown in Table 2.11: first column is the end-of-step position of the bank #10 in % of the withdrawal, second is the sum of reactivity introduced on this and previous steps and third is reactivity in pcm introduced per % of bank movement.

Table 2.11 Measurements of the integral and differential worth of control rod bank #10

H10, %	ΣΔρ, pcm	Δρ/ΔH, pcm/%	Tin, °C	P, MPa
0	0	0.00		
7	10	1.4		
13	22	2.0		
20	46	3.4		
26	95	8.2		
31	134	7.8		
37	192	9.7	280.0	15.87
43	251	9.8		
49	298	7.8		
56	347	7.0		
62	385	6.3		
68	415	5.0		
72	428	3.3		

3 Serpent 2 solution of the HZP X2 VVER-1000 benchmark

The fresh core HZP start-up experiments can be modelled by stand-alone Monte Carlo codes and are practically free from uncertainties associated with fuel burnup and thermal hydraulic feedbacks, which make these experiments very suitable for Monte Carlo code validation. Comparison of the Monte Carlo results with the measurements also allows verifying the consistency of the benchmark specification, accuracy of the model and applied nuclear data library. At the same time, the power distribution at the HZP state was not measured, so the Monte Carlo solution can be used as a reference for the verification of deterministic core simulators.

In this work fresh core HZP start-up experiments were modelled using the Serpent 2.1.31 Monte Carlo code (Leppänen et al., 2015). The cross section data applied is based on the ENDF/B-VII.0 evaluation (Chadwick et al., 2006).

3.1 Serpent model

The materials and geometry parameters of the fuel assembly models are directly adopted from the benchmark specifications. The dimensions of the model correspond to room temperature (i.e. thermal expansion is not taken into account). The only exception is the fuel active height which was expanded to 355 cm as described in section 2.1.2.

Since spacer grids and fuel cladding are composed from the same zirconium alloy, the spacer grid is modelled by increasing fuel rod cladding and control rod guiding tube thickness in corresponding axial layers (13 layers of a 2 cm height each in a fuel region and one more in an upper plenum region as illustrated in Fig. 2.15) to preserve the total mass of the alloy.

The Serpent model of the VVER-1000 core reproduces the benchmark specifications without any additional simplifications. The radial reflector model is limited by the inner surface of the reactor pressure vessel. The axial core periphery is defined in the benchmark and modelled in Serpent as homogeneously mixed layers. The high-resolution geometry plots of the Serpent model are available in an embedded dataset. In Serpent calculations, black boundary conditions are applied on the inner radius of the RPV and on the outer planes of the axial reflector.

3.2 Results and discussion

The critical boric acid concentration, temperature reactivity coefficients and control rod worth were measured in fresh core HZP conditions (see section 2.4.2). The experiments are simulated with Serpent and compared with measurements. The measurements uncertainties (where available) are shown as in the benchmark specification, which in turn were taken from NPP reports. The indicated uncertainty of Serpent results corresponds to one standard deviation of Serpent multiplication factor estimator and does not includes uncertainties of a model and applied nuclear data library. The reactivity coefficients and control rod worth are calculated as a reactivity difference between two corresponding Serpent criticality calculations:

$$\Delta\rho = \frac{1}{k_2} - \frac{1}{k_1}$$

where k_1 and k_2 – Serpent keff for two states before and after control rod movement or temperature change, respectively. The uncertainty of $\boldsymbol{\Delta\rho}$ is calculated as

$$\sigma_{\Delta\rho} = \sqrt{\sigma_1^2 + \sigma_2^2}$$

where σ_1 and σ_2 – standard deviations of Serpent keff for two states.

Critical state

For the stable critical state, the inlet coolant temperature was equal to 281.0 °C and the CB concentration was equal to 6.9 g/kg (1207 ppm). The control rod bank #10 was withdrawn to 76% and all other control rod banks were fully withdrawn (see Table 2.8).

For these conditions, keff calculated by Serpent is equal to 1.00012 ± 0.00001 which is very close to criticality. As shown in Table 3.1, the excess reactivity of 12 pcm can be compensated by additional

0.006 g/kg (1 ppm) of boric acid, so the estimated critical boron concentration in Serpent calculation is 6.906 g/kg (1208 ppm).

Table 3.1 Critical state

CB	Serpent keff
Measured: 6.900 g/kg (1207 ppm)	1.00012 ± 0.00001
Calculated: 6.906 g/kg (1208 ppm)	1.00000 ± 0.00001

The power distribution at HZP critical state was not measured in the experiment. However, 3D assembly power distribution in 20 equal axial layers (between 0 and 355 cm, with 17.75 cm layer height) and axially averaged pin-wise power (normalised fission rate distribution, not taking into account gamma smearing) profiles were calculated by Serpent. The results of five independent Serpent runs, each simulating $48*10^9$ neutron histories, were averaged. The resulting standard deviations of an assembly layer and pin power are < 0.1%.

The Serpent results for normalised axially averaged fuel assembly power and radially averaged axial power are shown in Fig. 3.1. Although Serpent calculations were performed in full 360 degree geometry, the problem and results are 60 degree symmetric and therefore shown in 60 degree sector. In absence of thermal feedbacks and Xe/Sm poisoning, the radial power distribution in this core layout in shifted towards core periphery with assembly power peaking factor (maximum relative assembly power) equal 1.41. The axial power distribution has a typical cosine shape with axial power peaking factor (maximum of radially averaged relative core axial power) equal 1.54.

The 3D assembly power distribution and axially averaged the pin-wise power profiles calculated by Serpent are included into the linked dataset for code-to-code comparison.

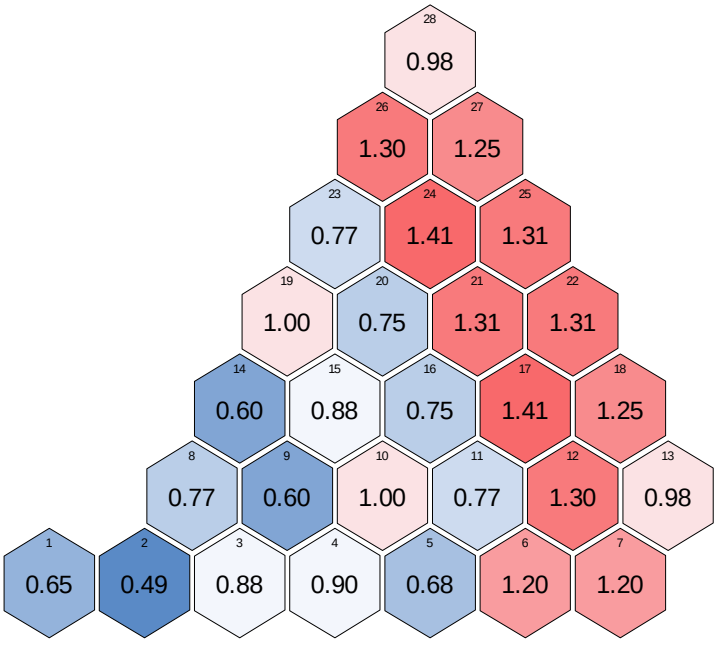

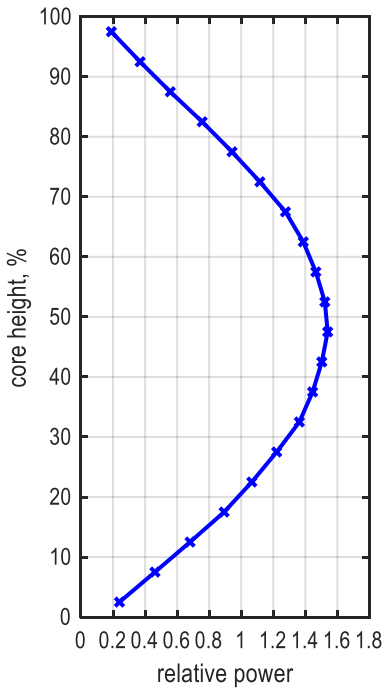

Fig. 3.1 Normalized power distribution

Temperature reactivity coefficient

The temperature reactivity coefficients were measured in two experiments with different control rod position and boron concentration, during temperature decrease and increase. Since there is no physical reason for temperature reactivity coefficient to be different on temperature decrease and increase, only a single value of temperature reactivity coefficient was obtained with Serpent for every experiment. The measured and calculated temperature reactivity coefficients, compared in Table 3.2, are in a reasonably good agreement. However, for every experiment, the corresponding measured values differ by about 10%. This variation can be partially attributed to uncertainty on reported operating conditions during the measurements, in particular coolant temperature and boron concentration. The assessment of sensitivity of temperature reactivity coefficients to variations in operating conditions is planned for the future.

Table 3.2 Temperature reactivity coefficient

	CB, g/kg	Δρ/ΔT, pcm/°C		
		Tin, °C	Experiment	Serpent
First measurement	7.05	280.7-276.0	-4.88±0.50	-5.60±0.3
		276.4-280.6	-5.39±0.54	
Second measurement	5.70	280.3-275.7	-13.58±0.14	-14.63±0.3
		275.7-280.2	-14.67±0.15	

SCRAM worth

Comparison of Serpent results with SCRAM worth experiment is shown in Table 3.3.

Table 3.3 SCRAM worth

	Δρ, pcm	
	Experiment	Serpent
SCRAM with a stuck rod	5230±310	5750±2
Full SCRAM	7000±430	7570±1

In both cases, Serpent overestimates the SCRAM worth by more than 500 pcm, which is about 8% of the full SCRAM worth. The systematic deviation between predicted and measured values of SCRAM worth is a known issue for VVER-1000 units, e.g. in (Bikeev et al., 2018) deviation of Monte Carlo predicted SCRAM worth from experiment was about 10%. The (Afanasiev and Pinegin, 2014) explained this deviation as a limitation of applied measurement technic. More specifically, the methodology behind reactimeter assumes asymptotic flux shape. However, this assumption is not valid in case of rapid introduction of high negative reactivity and leads to a systematic underestimation of the introduced reactivity. The (Afanasiev and Pinegin, 2014) and (Matveenko et al., 2010) proposed a modified experimental-computational methods of the SCRAM worth measurement, where point kinetics equation is modified with per-calculated time-dependent correction factors for adjoin flux, beta effective and ratio between reactor power and ionization chamber

current. Proposed methods were implemented and tested at few VVER-1000 units, showing a clearly improved agreement between measurement and numerical simulations.

Another reason for deviations between SCRAM worth measurement and Serpent results is the fact that dynamic process was simulated by static calculations, which is not a fair comparison (Cullen et al., 2003). More consistent simulation of the experiment can be performed using a space-time kinetics code with a capability to predict the ex-core detector/ionization chamber response.

Differential and integral worth of control rod bank #10

The measurement control rod (CR) bank #10 differential worth starts from all banks fully out and bank #10 fully in. During measurement boron concentration is continuously increasing and bank #10 is step-wise withdrawn and the introduced reactivity is measured in each step. Comparison of Serpent results with experiment is shown in Table 3.4 and in Fig. 3.2. The **H10** in Table 3.4 is the end-of-step position in % of the withdrawal, **Δρ** is a reactivity in pcm introduced in step and **Δρ/ΔH** is reactivity in pcm introduced per % of bank movement. Measurement uncertainty for this experiment is not available.

Table 3.4 Differential and integral worth of CR bank #10

H10, %	Δρ, pcm		Σ Δρ, pcm		Δρ/ΔH, pcm/%	
	Experiment	Serpent	Experiment	Serpent	Experiment	Serpent
0	0	0	0	0	-	-
7	10	6±1	10	6±1	1.4	0.8±0.2
13	12	15±1	22	20±2	2.0	2.4±0.2
20	24	30±1	46	50±2	3.4	4.2±0.2
26	49	37±1	95	87±2	8.2	6.2±0.2
31	39	40±1	134	127±2	7.8	8.0±0.3
37	58	51±1	192	178±3	9.7	8.5±0.2
43	59	52±1	251	230±3	9.8	8.7±0.2
49	47	49±1	298	279±3	7.8	8.1±0.2
56	49	50±1	347	330±3	7.0	7.2±0.2
62	38	35±1	385	364±3	6.3	5.8±0.2
68	30	30±1	415	395±3	5.0	5.1±0.2
72	13	17±1	428	412±4	3.3	4.2±0.4

Comparison of experimental and calculated differential worth in Fig. 3.2 demonstrates good overall agreement except few points in a central part, where Serpent results are significantly lower than measurement. At the same time, measured data points do not fit into expected smooth curve, which clearly suggest high uncertainty of the measurement. The integral worth (Fig. 3.3 s-curve) accumulates errors of each step – so the total worth calculated by Serpent is about 4% (16 pcm) less than measured. Apart from measurement uncertainties, the possible reason for deviation can be an uncertainty in a CR model. In particular, the fuel specification documents indicate minimal required density of the absorbing materials, which was accepted for a benchmark specification. In reality, however, these densities are not known exactly and might be slightly higher.

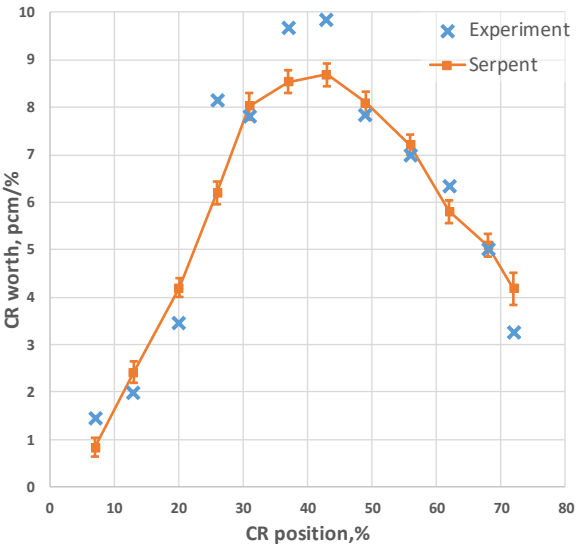

Fig. 3.2 Differential worth of bank #10

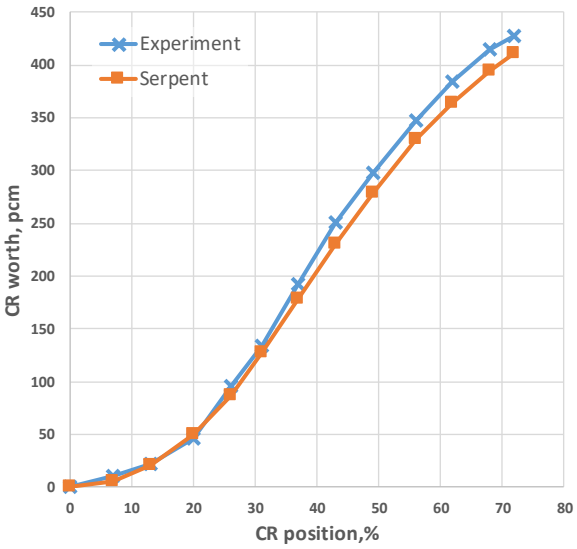

Fig. 3.3 Integral worth of bank #10

4 Summary and future work

This paper presents a revision of the X2 benchmark which is based on the operational data of the VVER-1000 core of the Unit 2 of the Khmelnitsky NPP. The paper focuses on the fresh core HZP tests and includes a detail description of core geometry, material compositions, description and results of measurements performed during the fresh core start-up. The new revision features more detailed reflector specifications, descriptions of experimental procedures, and several updates and corrections of benchmark specifications.

The benchmark data was also compiled into a linked online dataset and include spreadsheets with operational conditions and material compositions, high resolution geometry drawings, and other information. The new revision comprises a unique dataset for validation of reactor simulation codes employed for VVER analyses.

Moreover, the paper presents the Monte Carlo reference solution for the HZP fresh core states obtained with the Serpent 2 code applying the ENDF/B-VII.0 evaluated nuclear data library. The calculated CB concentration, temperature reactivity coefficients, SCRAM worth, and integral and differential worth of the CR #10 were compared with the measured values.

The CB concentration predicted by Serpent agrees within 1 ppm with the measured data. However, the application of alternative cross section libraries can lead to slightly different results.

The temperature reactivity coefficients estimated by Serpent are in a reasonably good agreement with the experimental values while measurement uncertainties seem to be underestimated.

Serpent noticeably overestimated the SCRAM worth by more than 500 pcm. The deviation can be explained by known limitations of applied measurement methodology. An improved measurement method is been implemented in VVER-1000 units.

The calculated and measured differential worth of the CR Bank 10 are in a good agreement except few points in a central part. On one hand, the uncertainty of measured data is high; on the other hand, deviations might result from uncertainty of a CR model, in particular, density of absorbing material. The integral worth of the CR Bank 10 calculated by Serpent is 4% less than measurement.

Although, the benchmark does not provide the measured power distribution at HZP critical state, 3D assembly power distribution and axially averaged the pin-wise power profiles were calculated by Serpent and were included into the linked dataset. This information is can be used for code-to-code comparisons.

In the near future, it is planned to repeat the HZP analysis with alternative nuclear data evaluations and supplement it with the nuclear data sensitivity and uncertainty studies. Extending the X2 benchmark specification with operational history data and HZP tests of the 2^{nd} - 4^{th} fuel cycles as well as operational transients is also foreseen.

References

AER [WWW Document], 2019. http://www.aer-web.com/

Afanasiev, D.V., Pinegin, A.A., 2014. The practice of considering reactivity spatial effects when measuring emergency protection efficiency in VVER reactors, in Proc.: 24th Symposium of AER on VVER Reactor Physics and Reactor Safety, Sochi, Russia.

Bahadir, T., 2018. SIMULATE5-HEX extension for VVER analyses. Kerntechnik 83, pp. 268–274.

Bikeev, A., Kalugin, M., Shcherenko, A., Shkarovsky, D., 2018. Simulation of VVER-1000 startup physics tests using the MCU Monte Carlo code. Annals of Nuclear Energy 117, pp. 60–66.

Bilodid, Y., Grundmann, U., Kliem, S., 2018. The HEXNEM3 nodal flux expansion method for the hexagonal geometry in the code DYN3D. Annals of Nuclear Energy 116, pp. 187–194.

Chadwick, M.B., Obložinský, P., Herman, M., Greene, N.M., McKnight, R.D., Smith, D.L., Young, P.G., MacFarlane, R.E., Hale, G.M., Frankle, S.C., Kahler, A.C., Kawano, T., Little, R.C., Madland, D.G., Moller, P., Mosteller, R.D., Page, P.R., Talou, P., Trellue, H., White, M.C., Wilson, W.B., Arcilla, R., Dunford, C.L., Mughabghab, S.F., Pritychenko, B., Rochman, D., Sonzogni, A.A., Lubitz, C.R., Trumbull, T.H., Weinman, J.P., Brown, D.A., Cullen, D.E., Heinrichs, D.P., McNabb, D.P., Derrien, H., Dunn, M.E., Larson, N.M., Leal, L.C., Carlson, A.D., Block, R.C., Briggs, J.B., Cheng, E.T., Huria, H.C., Zerkle, M.L., Kozier, K.S., Courcelle, A., Pronyaev, V., van der Marck, S.C., 2006. ENDF/B-VII.0: Next Generation Evaluated Nuclear Data Library for Nuclear Science and Technology. Nuclear Data Sheets 107, pp. 2931–3060.

Cullen, D.E., Little, R., Procassini, R., Clouse, C., 2003. Static and Dynamic Criticality: Are They Different? LLNL UCRL-TR-201506.

Ivanov, B., Ivanov, K., Groudev, P., Pavlova, M., Hadjiev, V., 2002. VVER-1000 Coolant Transient Benchmark PHASE 1 (V1000CT-1) Vol. I: Main Coolant Pump (MCP) switching On - Final Specifications. NEA/NSC/DOC(2002)6.

Krýsl, V., Mikoláš, P., Sprinzl, D., Švarný, J., 2016. PROPOSAL OF "FULL-CORE" VVER-1000 CALCULATION BENCHMARK, in Proc.: Proc. of the 26th Symposium of AER on VVER Reactor Physics and Reactor Safety, Helsinki, Finland.

Leppänen, J., Pusa, M., Viitanen, T., Valtavirta, V., Kaltiaisenaho, T., 2015. The Serpent Monte Carlo code: Status, development and applications in 2013. Annals of Nuclear Energy 82, pp. 142–150.

Lötsch, T., 2014. Fuel assembly burnup calculations for VVER fuel assemblies with the MONTE CARLO code SERPENT. Kerntechnik 79, pp. 295–302.

Lötsch, T., Khalimonchuk, V., Kuchin, A., 2013. Consolidated Data for the Task 2 of the VVER-1000 Core Burnup Benchmark, in Proc.: Proceedings of the 23. Symposium of AER, Štrbské Pleso, Slovakia.

Lötsch, T., Khalimonchuk, V., Kuchin, A., 2012. Consolidated data for task1 and status of task 2 of the benchmark for core burnup calculations for a VVER-1000 reactor, in Proc.: Proceedings of the 22. Symposium of AER, Pruhonice, Czech Republic.

Lötsch, T., Khalimonchuk, V., Kuchin, A., 2010. Corrections and additions to the proposal of a benchmark for core burnup calculations for a VVER-1000 reactor., in Proc.: Proceedings of the 20th AER Symposium on VVER Reactor Physics and Reactor Safety, Hanasaari, Espoo, Finland.

Lötsch, T., Khalimonchuk, V., Kuchin, A., 2009. Proposal of a benchmark for core burnup calculations for a VVER-1000 reactor core., in Proc.: Proceedings of the 19th AER Symposium on VVER Reactor Physics and Reactor Safety, St. St. Constantine and Elena Resort, Bulgaria.

Lötsch, T., Kliem, S., Bilodid, E., Khalimonchuk, V., Kuchin, A., Ovdienko, Y., Ieremenko, M., Blank, R., Schultz, G., 2016. The X2 benchmark for VVER-1000 reactor calculations. Overview and current status., in Proc.: Proceedings of the 26th AER Symposium on VVER Reactor Physics and Reactor Safety, Helsinki, Finland.

Matveenko, I.P., Lititskii, V.A., Shokod'ko, A.G., 2010. Consideration of spatial effects in reactivity measurements. Physics of Atomic Nuclei 73, pp. 2209–2213.

Novak, O., Chvala, O., Luciano, N.P., Maldonado, G.I., 2017. VVER 1000 Khmelnitskiy benchmark analysis calculated by Serpent2. Annals of Nuclear Energy 110, pp. 948–957.

Tereshonok, V.A., Nikonov, S.P., Lizorkin, M.P., Velkov, K., Pautz, A., Ivanov, K., 2009. Kalinin-3 coolant transient benchmark –switching-off of one of the four operating main circulation pumps at nominal reactor power.